Density and Temperature Sensitive Features in High Temperature Plasma L-Shell Xenon Emission Spectra

C. J. Keane, B. A. Hammel, A. L. Osterheld, and D. R. Kania
Lawrence Livermore National Laboratory, University of California, Livermore, California 94550
(Received 22 February 1993)

We present model calculations demonstrating new density and temperature sensitive ratios of groups of F- and Ne-like Xe lines which are suitable for diagnosing plasma conditions. The method is illustrated by using L-shell Xe emission to infer T_e in the fuel region of indirectly driven plastic capsules filled with deuterium and doped with 0.1% Ar and 0.02% Xe. The technique uses tractable atomic models and appears scalable to other Ne-like ions.

PACS numbers: 52.25.Nr, 52.50.Jm

Methods of inferring T_e in high temperature plasmas based on emission spectroscopy have been extensively discussed in the literature [1]. To date these methods rely on either the ratio of two individual spectral lines or the slope of free-bound recombination continua. Furthermore, most of the methods discussed to date use K-shell ions due to their simple atomic structure.

In this Letter we describe new temperature and density sensitive spectral features in the L-shell spectra of highly ionized Xe suitable for inferring diagnostic information regarding T_e and N_e in non-LTE (local thermodynamic equilibrium) plasmas. These spectral features consist of many individual lines from Mg- through F-like Xe. The relatively large wavelength extent of these features implies that only modest instrumental resolution is required.

While the method is applicable to L-shell ions in general, we focus on Xe here as it is of interest for diagnosing plasma conditions in the gaseous fuel region of inertial confinement fusion (ICF) targets. Indeed, Ne-like Xe emission has been observed from such targets [2] and the feasibility of using Stark broadening of Xe 3-2 and 4-2 transitions as electron density diagnostics has also been explored [3]. The development of high photon energy ($h\nu \sim 4$–7 keV) spectral diagnostics of this type also provides a means of diagnosing fuel conditions in high performance implosions characterized by pusher opacities too high to allow normal Ar and Cl emission to be used [4,5].

Diagnostics of T_e and N_e based on the ratio of individual lines in Ne-like ions have been previously reported [6,7]. Variations in the relative intensity of broad emission spectral features of the type discussed here as a function of laser and plasma conditions have also been observed [8]. In this work the behavior of a class of such spectral features is quantified in the non-LTE regime and shown to be sensitive to both T_e and N_e, thus opening up diagnostic applications. This is possible because we are considering emission from ion stages near the relatively simple closed shell Ne-like ion, which allows the emission to be treated explicitly with a detailed model as opposed to an approximate LTE unresolved transition array (UTA) technique required for more complex emitters [9]. Detailed non-LTE calculations typical of laboratory conditions can thus be carried out and temperature and density sensitive spectral ratios identified.

The diagnostic technique described here is most easily seen by considering a detailed non-LTE calculation of the kinetics of Xe for $T_e = 2$ keV and $N_e = 10^{24}$ cm^{-3}, conditions typical of the fuel region in current ICF targets [4,5]. Under these conditions Xe is ionized to near the Ne-like stage, and hence a detailed model for Xe in this region of ionization was constructed for these calculations using methods described elsewhere [10]. The model includes singly excited levels through $n = 10$ for N-like (Xe^{47+}) through Si-like (Xe^{41+}) xenon; within each possible core configuration levels with $n \geq 4$ are treated as a single level. All singly excited levels are treated in a configuration average approximation with the exception of the Ne-like $n = 3$ manifold, where fine structure is used (i.e., all 36 excited states are considered individually). For Na-, Mg-, and Ne-like Xe, all $3l3l'$ autoionizing levels are considered, once again in a configuration average approximation. The model is input to a collisional-radiative solver which computes populations and produces synthetic spectra [10]. In calculating line spectra, all configuration averaged levels are broken out into their fine structure components (with corresponding energies). Levels within a configuration are then populated according to their statistical weight. All calculations are carried out in the steady state, optically thin limit, which provides a demonstration of the technique.

The main result of these calculations is shown in Figs. 1(a) and 1(b), where synthetic spectra for Xe are shown at $N_e = 10^{24}$ cm^{-3} for $T_e = 2$ and 1.4 keV, respectively. This relatively small change in electron temperature changes the spectrum significantly. In addition to the Ne-like $2s$-$3p$ line at 2.46 Å [denoted "$3A$" in Fig. 1(a)], two features consisting of blends of many lines become visible at higher temperature. These are (I) F- and Ne-like emission from 2.49 to 2.53 Å, including the $2s$-$3p$ Ne-like resonance line at 2.50 Å, and (II) F- and Ne-like emission from 2.64 to 2.7 Å. These features consist of F-like $2p$-$3d$ resonance lines (a number of which have been observed [2]) as well as Ne-like *satellite* transitions

0031-9007/94/72(19)/3029(4)$06.00

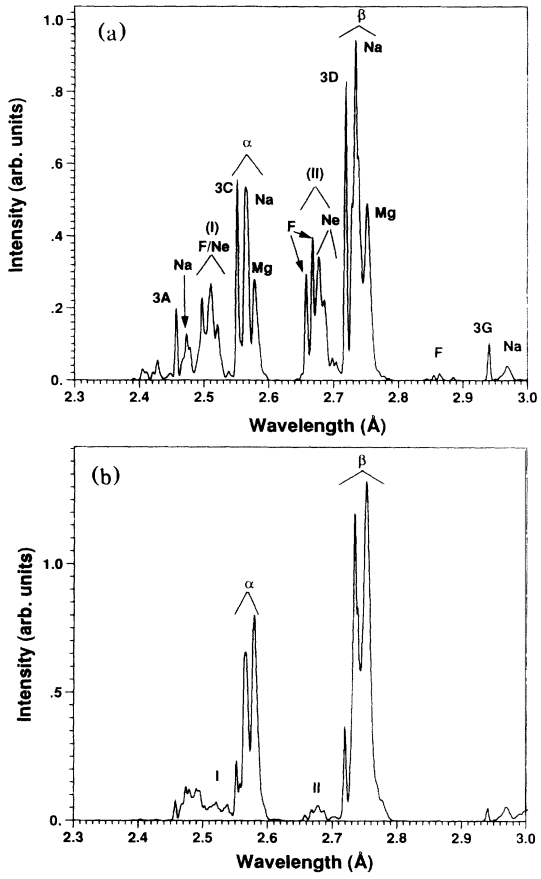

FIG. 1. Calculated Xe spectra for (a) $T_e=2$ keV, $N_e=10^{24}$ cm^{-3} and (b) $T_e=1.4$ keV, $N_e=10^{24}$ cm^{-3}. A FWHM of 0.004 Å was assumed for each individual spectral line.

with $3l3l'$ upper states. The Ne-like satellites included in the model consist of $2p$-$3d$, $2p$-$3s$, and $2s$-$3p$ transitions in the presence of $3s$, $3p$, or $3d$ spectator electrons, e.g., $1s^22s^22p^53s$-$1s^22s^22p^43s3d$. The longer wavelength $2s$-$3p$ resonance line at 2.50 Å is also included in feature I. In feature II, the F-like resonance lines run mainly from 2.65 to 2.67 Å, while the region 2.67 to 2.7 Å consists primarily of Ne-like satellites.

Before proceeding further we note that a Gaussian line shape with full width at half maximum (FWHM) of 0.004 Å was assumed for each radiative transition in Fig. 1, which corresponds roughly to the Doppler width at $T_i=1$ keV. The use of Doppler broadening is based on calculations which show that pressure broadening is negligible for the Ne-like Xe $n=3$ manifold for the densities considered here ($N_e \leq 10^{24}$ cm^{-3}) [3]. It was found that the diagnostic line ratios to be described do not change as the assumed FWHM is varied within reason. In addition, simple estimates [11] show that at the highest N_e considered ($N_e=10^{24}$ cm^{-3}) levels up to $n=8$ are not affected by continuum lowering, and hence this effect was neglected.

Features I and II are of interest due to their relatively large width which makes them easily observable with

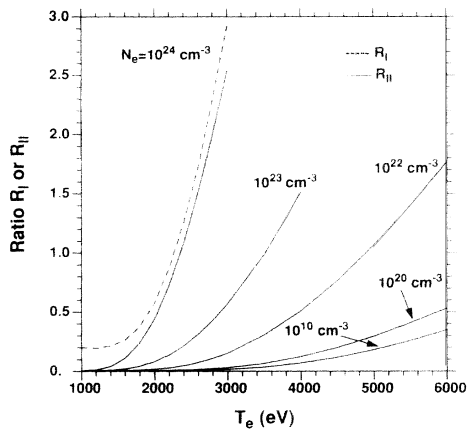

FIG. 2. Ratios R_I (dashed) and R_{II} (solid) vs T_e at different electron densities. Referring to Fig. 1, $R_I=I/A$ and $R_{II}=II/B$.

spectrometers of moderate spectral resolution. Analysis shows that upper states of the Ne-like satellites in features I and II are populated primarily by dielectronic recombination as opposed to inner shell excitation. Thus, the intensity of features I and II is primarily proportional to the F-like ground state population, and the ratio of features I and II to nearby Mg-, Na-, and Ne-like emission should vary with T_e and N_e as the relative ionization balance. We denote the nearby Ne-, Na-, and Mg-like emission for features I and II by "α" and "β," respectively, as shown in Fig. 1(a). This grouping corresponds to what is typically seen experimentally in spectra from plasmas ionized near the Ne-like stage.

Figure 2 shows the ratio $R_I=I/\alpha$ and $R_{II}=II/\beta$ vs T_e at $N_e=10^{24}$ cm^{-3}. [Each curve in Fig. 2 is stopped at the highest T_e appropriate to insure the validity of the calculation by making sure that the highest ion stage considered (N-like) in the model is relatively weakly populated.] The variation in ionization balance with T_e over the same temperature range for $N_e=10^{24}$ and 10^{10} cm^{-3} is shown in Figs. 3(a) and 3(b). The increase in R_I and R_{II} with T_e follows the relative increase in the F-like fraction shown in Figs. 3(a) and 3(b). Finally, the "floor" in R_I at low T_e is due to Na- and Mg-like satellites to the $2s$-$3p$ Ne-like resonance lines.

Figure 2 shows a dependence on N_e for R_{II} (a similar behavior holds for R_I). This arises due to stepwise ionization effects. Figures 3(a) and 3(b) show this clearly; as N_e is decreased below 10^{24} cm^{-3} a higher T_e is needed to produce a given F-like fraction. At lower densities and at the higher temperatures needed to produce a given F-like fraction, R_I and R_{II} are reduced because the necessary elevated T_e reduces the intensity of Ne-like satellites and increases the brightness of Ne-like resonance lines. Figure 3(c) further illustrates these conclusions by showing the average ion charge vs N_e. It is apparent that stepwise ionization effects are important for $N_e \gtrsim 10^{20}$ cm^{-3} [equivalently, Fig. 3(b) is essentially the same for $10^{10} < N_e < 10^{20}$ cm^{-3}]. Figure 3(c) also shows that for $N_e \gtrsim 10^{24}$ cm^{-3} the plasma ionization decreases with in-

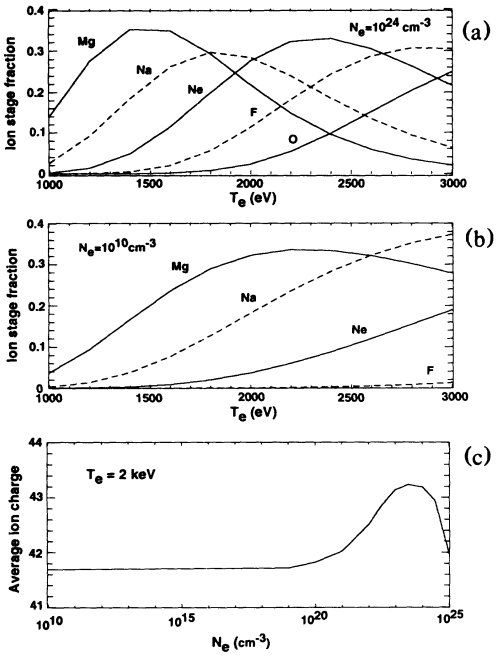

FIG. 3. (a) Calculated Xe ion fractions vs T_e for $N_e=10^{24}$ cm^{-3}. (b) Same as (a) but for $N_e=10^{10}$ cm^{-3}. (c) Average Xe ion charge vs N_e for $T_e=2$ keV.

creasing electron density and approaches the LTE limit.

We next consider the importance of excitation-autoionization and dielectronic recombination. Figure 4 shows the F-like fraction vs T_e at $N_e=10^{24}$ cm^{-3}, and shows that dielectronic recombination and excitation autoionization play comparable roles in determining the F-like fraction (and therefore $R_{\rm I}$ and $R_{\rm II}$). $R_{\rm I}$ and $R_{\rm II}$ were found to vary by 10%–20% when excitation autoionization was neglected.

The effects of differing levels of complexity in the atomic model have also been considered. Previous work [10] has shown that treating the $n=3$ manifold in Ne-like ions in a fully detailed level accounting scheme as opposed to a configuration average approximation can affect the ionization balance significantly. This is especially true at intermediate densities (such as in x-ray laser plasmas [10,12]), where the density is high enough to appreciably populate metastable levels (such as the $3p$ manifold in Ne-like ions) but not large enough to collisionally mix their population with nearby nonmetastable levels. At $N_e=10^{24}$ cm^{-3} $R_{\rm I}$ and $R_{\rm II}$ were found to vary by 5%–10% when the $n=3$ manifold in Ne-like Xe was treated with a configuration average model as opposed to a detailed level accounting treatment. This difference increased to 30%–40% at $N_e=10^{20}$ cm^{-3}, presumably due to the decreased importance of collisional mixing. Care should be taken when using $R_{\rm I}$ and $R_{\rm II}$ for $N_e \lesssim 10^{20}$ cm^{-3} due to the increased error in the inferred T_e and/or N_e arising from this effect.

Before turning to a sample application of this technique we discuss three final points. First, the model used

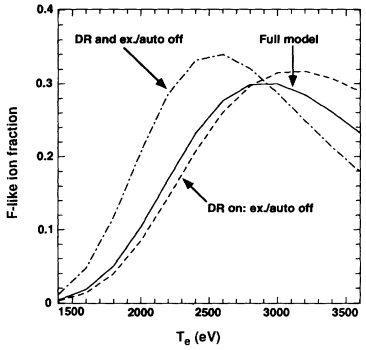

FIG. 4. F-like ion fraction vs T_e at $N_e=10^{24}$ cm^{-3} for differing atomic models. Solid: Full model. Dashed: Full model with dielectronic recombination but no excitation autoionization. Dot-dashed: Full model with no dielectronic recombination and no excitation autoionization.

here consists of 559 singly excited and 298 autoionizing levels. While not small, this is of sufficiently moderate size to be used on personal computers or as part of a hydrodynamic postprocessing code. Hence, the method is accessible. Second, this method should be scalable to any Ne-like ion, although this remains to be verified. A limiting factor may well be line overlaps; as Z decreases the wavelength spacing between the $3C$ and $3D$ lines is reduced, making feature II more difficult to resolve. Finally, as can be seen from Fig. 2 $R_{\rm I}$ and $R_{\rm II}$ are sensitive to both T_e and N_e. However, in most laboratory plasmas one of these quantities is known well enough so that $R_{\rm I}$ and $R_{\rm II}$ may be used to estimate the other. This is typically true for ICF targets, where x-ray imaging and nuclear diagnostics yield the fuel density quite accurately; $R_{\rm I}$ and $R_{\rm II}$ may then be used to estimate T_e.

We now illustrate this technique by using it to estimate T_e in the fuel region of capsules indirectly imploded using the Nova laser [4,5]. In these experiments 0.35-μm laser light in a 1-ns square pulse is directed into a 2550-μm-long by 1600-μm-wide gold hohlraum with 800-μm-wide laser entrance holes. The laser light is converted to x rays which are then used to implode a plastic capsule with inner diameter and total wall thickness of 440 μm and 70 μm, respectively. We will consider experiments carried out with either 28 kJ ("high drive") or 19 kJ ("nominal drive") of laser light, which corresponds to peak drive temperatures of approximately 260 and 220 eV. The fuel mixture consisted of deuterium at 50 atm pressure with 0.1% Ar and 0.02% Xe by atom number. (The capsule hydrodynamic behavior as calculated by LASNEX [13] is not perturbed by addition of Ar and Xe dopants at this level.) The flat crystal streaked x-ray spectrograph used to record the Xe spectra had a spectral resolving power ($\lambda/\Delta\lambda$) of 500 [5]. We will focus here on comparisons of the fuel T_e inferred from Xe spectroscopy for the nominal and high drive cases.

Figure 5 shows sample Xe spectra in the 3-2 region at time of peak emission for the nominal and high drive

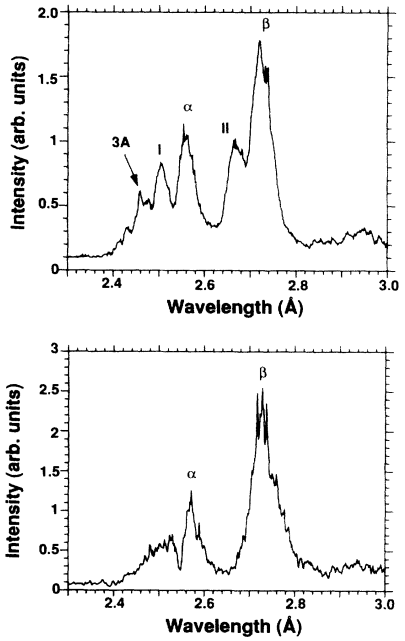

FIG. 5. Observed Xe spectra at time of peak emission from high (top) and nominal (bottom) indirect drive implosions.

cases. The actual peak drive temperatures for these shots were 258 and 223 eV. Comparing Fig. 5 to Figs. 1(a) and 1(b) shows that features I and II in Fig. 1(a) are present for the high drive case and not observed at nominal drive. Note that the Ne-like $3A$ line is weakly observed at high drive. Applying a curve fitting procedure to the I, II, α, and β features in the high drive case yields $R_{\rm I}=0.4\pm0.1$ and $R_{\rm II}=0.34\pm0.05$. From Fig. 2 this corresponds to electron temperatures of 1.8 ± 0.2 and 1.9 ± 0.1 keV, respectively. (The fuel N_e was measured to be 10^{24} cm^{-3} from Stark broadening of Ar Ly-β [4, 5].) For the nominal drive case the absence of features I and II implies that $T_e \lesssim 1400$ eV. These results compare with volume averaged electron temperatures of 1.6 keV (high drive) and 1.2 keV (nominal drive) obtained from the ratio of Ar Ly-β to He-β on similar shots, which are in good agreement with LASNEX simulations [4,5]. Finally, we note that the intensity of the α and β features should not be affected by opacity, as the $3C$ and $3D$ $2p$-$3d$ Ne-like resonance lines with depths of a few are the only optically thick lines present.

A full comparison to the data in Fig. 5 would require a detailed kinetics and radiative transfer calculation, including the effects of gradients; however, the data and analysis as given provide evidence for validity of the technique described here. Note that by comparing Fig. 5 and Fig. 1(a), given the instrumental resolving power of 700 [approximately equivalent to the assumed width of 0.004 Å in Fig. 1(a)], more detail would be expected in the spectra of Fig. 5. The fact that the spectra in Fig. 5 do not show more features indicates that there are probably other phenomena present, such as unaccounted for transitions or line broadening effects. Our future work in this area thus involves both higher resolution spectral measurements and more detailed modeling that includes spatial gradients in T_e and N_e.

This work was performed under the auspices of the U.S. Department of Energy by the Lawrence Livermore National Laboratory under Contract No. W-7405-ENG-48.

[1] R. L. Kauffman, in *Physics of Laser Plasma*, Handbook of Plasma Physics Vol. 3, edited by A. Rubenchik and S. Witkowski (North-Holland, Amsterdam, 1991).

[2] Y. Conturie, B. Yaakobi, U. Feldman, G. A. Doschek, and R. D. Cowan, J. Opt. Soc. Am. B **71**, 1309 (1981).

[3] C. J. Keane, R. W. Lee, B. A. Hammel, A. L. Osterheld, L. J. Suter, A. Calisti, F. Khelfaoui, R. Stamm, and B. Talin, Rev. Sci. Instrum. **61**, 2780 (1990).

[4] C. J. Keane, B. A. Hammel, D. R. Kania, J. D. Kilkenny, R. W. Lee, A. L. Osterheld, L. J. Suter, R. C. Mancini, C. F. Hooper, Jr., and N. D. Delamater, Phys. Fluids B **5**, 3328 (1993).

[5] B. A. Hammel, C. J. Keane, M. D. Cable, J. D. Kilkenny, R. W. Lee, and R. Pasha, Phys. Rev. Lett. **70**, 1263 (1993); B. A. Hammel, C. J. Keane, D. R. Kania, J. D. Kilkenny, R. W. Lee, R. Pasha, and R. E. Turner, Rev. Sci. Instrum. **63**, 5017 (1992).

[6] W. H. Goldstein, R. Walling, J. Bailey, M. Chen, R. Fortner, M. Klapisch, T. Phillips, and R. Stewart, Phys. Rev. Lett. **58**, 2300 (1987).

[7] O. Peyrusse, P. Combis, M. Louis-Jacquet, D. Naccache, C. J. Keane, B. J. MacGowan, and D. L. Matthews, J. Appl. Phys. **65**, 3802 (1989).

[8] A. Zigler, M. Givon, E. Yarkoni, M. Kishinevsky, E. Goldberg, B. Arad, and M. Klapisch, Phys. Rev. A **35**, 280 (1987).

[9] J. Bauche, C. Bauche-Arnoult, and M. Klapisch, Adv. At. Mol. Phys. **23**, 131 (1987).

[10] A. L. Osterheld, B. K. F. Young, R. S. Walling, W. H. Goldstein, J. H. Scofield, M. Chen, G. Shimkaveg, M. Carter, R. Shepherd, B. J. MacGowan, L. Da Silva, D. Matthews, S. Maxon, R. London, and R. E. Stewart, in *Proceedings of the 3rd International Colloquium on X-Ray Lasers* (Institute of Physics, Bristol, 1992), pp. 309–314.

[11] R. M. More, J. Quantum. Spectrosc. Radiat. Transfer **27**, 345 (1982).

[12] For further information and references on x-ray laser modeling, see, for example, R. A. London, M. D. Rosen, M. S. Maxon, D. C. Eder, and P. L. Hagelstein, J. Phys. B **22**, 3363 (1989).

[13] G. B. Zimmerman and W. L. Kruer, Comments Plasma Phys. Controlled Fusion **2**, 51 (1975).